Large-scale atomistic simulation of diffusion in refractory metals and alloys

Sergei Starikov [1,*] Petr Grigorev,[2] Ralf Drautz [1] and Sergiy V. Divinski [3]

[1]*The Interdisciplinary Centre for Advanced Materials Simulation (ICAMS), Ruhr-Universität Bochum, 44801 Bochum, Germany*

[2]*Aix-Marseille Universite, CNRS, CINaM UMR 7325, Campus de Luminy, 13288 Marseille, France*

[3]*Institute of Materials Physics, University of Münster, 48149 Münster, Germany*

(Received 7 February 2024; accepted 28 March 2024; published 22 April 2024)

The equilibrium vacancy concentration and atomic diffusion coefficients in dilute and complex refractory alloys have been calculated using various computational methods. The most productive technique has been large-scale atomistic simulation in the form of a numerical experiment in which a crystal with free surfaces was simulated for a relatively long time. This method is based on the concept that the free surface acts as a source of point defects and provides a natural way to achieve an equilibrium concentration of the defects within the bulk after an initial annealing stage. For complex concentrated alloys (CCAs), this numerical experiment offers the possibility to study diffusion processes where standard analytical approaches are difficult to apply due to the large variety of microscopic states. As the simulation results, we found that the transition from dilute alloys to CCA is accompanied by a significant increase in atomic diffusion rate due to both a substantial increase in the vacancy concentration and their mobility.

DOI: 10.1103/PhysRevMaterials.8.043603

I. INTRODUCTION

Atomic diffusion is one of the most important processes in materials science, controlling the microstructure evolution during materials processing and heat treatment [1–3]. For most metals, the bulk diffusion of atoms is governed by the migration of vacancies. The tracer self-diffusion coefficient, D^* or D for simplicity, is determined as the product of the vacancy concentration, C_v, and the vacancy diffusion coefficient, D_v [2,4–6].

In the past decade, many interesting aspects of self-diffusion in pure metals with body-centered-cubic (bcc) and face-centered-cubic (fcc) lattices have been studied in detail, both experimentally and theoretically. For example, the well-known phenomenon of the non-Arrhenius temperature dependence of D^* at high temperatures [7–10] was explained by a dominant contribution of a strong temperature dependence of the vacancy formation energy E_v^f due to anharmonic effects [11–17]. In fact, this energy at the melting point can be 40% higher than the vacancy formation energy at zero temperature, E_{v0}^f. At the same time, many aspects of atomic diffusion in alloys remain poorly understood. In particular, the presence of a "sluggish diffusion effect" in high-entropy alloys (HEAs) or more generally in complex concentrated alloys (CCAs) is heavily debated [18].

The concept of sluggish diffusion was first formulated for fcc HEAs [19,20] and then generalized to bcc alloys [21,22] or even to B2 ordered alloys [23]. The basic idea is the existence of local atomic configurations that act as vacancy traps and suppress atomic diffusion. The sluggish diffusion of atoms in fcc CCAs has apparently been confirmed in a number of studies [20,24–26], but recent investigations revealed controversial behaviors for different elements in the same alloys [27] or the absence of diffusion retardation in many complex alloys [28–31]. Moreover, some theoretical works [32,33] predict that an enhancement of atomic diffusion in CCAs compared to dilute alloys is a more common phenomenon and this was experimentally documented later [31,34].

The most powerful method of diffusion measurements is based on the tracer diffusion (tracing of radioactive markers) [35] and it was intensively applied to HEAs generating reliable mobility databases for all elements, especially for fcc CoCrFeMnNi alloy [27,36–38]. Even composition-dependent tracer diffusion coefficients were determined [39]. Less information is available for HEAs with other crystalline lattices, such as bcc [31], hexagonal close packed (hcp) [34,40,41], or sigma [42] lattices. These results have relativized the original concept of "sluggish" diffusion in HEAs, demonstrating that element mixing may result in some retardation of the diffusion rates in fcc CoCrFeMnNi (e.g., of Ni but not of Mn) [27], slight enhancement of those in bcc HfTiZrTaNb [31], or even significant increase of the tracer diffusion coefficients in hcp AlScHfTiZr [34]. For further details of the tracer diffusion measurements, the reader is referred to the recent overviews in, e.g., Refs. [18,28]. However, even these difficult and expensive experiments provide the resulting values of the element-specific diffusion coefficients without required details about the different contributions in the diffusion process, i.e., the vacancy concentration, vacancy–element binding, correlation effects, etc. Thus atomistic modeling plays a key role in understanding the underlying mechanisms of atomic diffusion [13,43–45].

In this work, we used several computational methods to study details of atomic diffusion in dilute and CCAs based on the W–Mo–Nb ternary system. Among other approaches,

*sergei.starikov@icams.rub.de

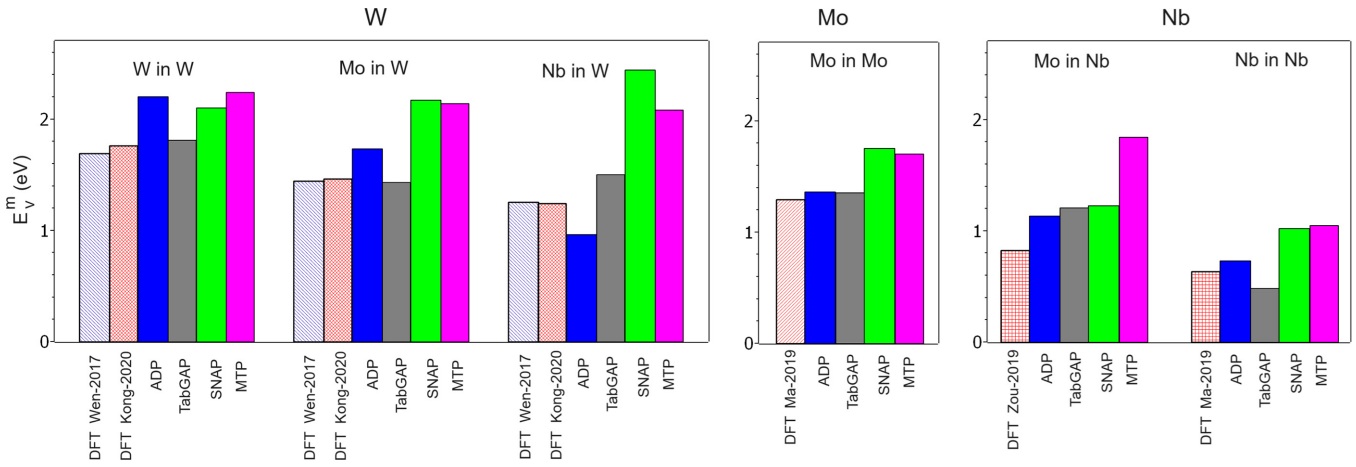

FIG. 1. Calculated migration energies for the alloying atom moving by exchange with the vacancy. Available DFT data [5,6,43,44] are compared with the results obtained from the ADP [47], tabGAP [55], SNAP [53], and MTP [54] models.

we used large-scale molecular dynamics (MD) simulation, which is performed in the form of a numerical experiment. Namely, a relatively large crystal with two free surfaces was simulated for 10–50 nanoseconds at a given temperature. The free surface acts as a source of point defects and provides a natural way to achieve an equilibrium concentration of the defects in the bulk. Previously, this approach has been used to study many diffusion phenomena in pure metals [13,45,46] and here we apply it to study bulk atomic diffusion in alloys.

The paper is organized as follows. The simulation methods are described in Sec. II. In Sec. III, we discuss the diffusion and formation energy of a single vacancy. Section IV presents the large-scale simulation results. Section V is devoted to a final discussion.

II. COMPUTATIONAL METHODS

This study aims to investigate the diffusion in dilute and complex concentrated alloys based on the W-Mo-Nb ternary system. For the purpose of this work, we used different computational methods based on static and MD simulations. The variety of approaches makes it possible to obtain a more detailed description of the phenomenon studied and to double-check the results.

A. Interatomic potential

The key aspect of a classical atomistic simulation is the choice of the interatomic potential. Recently we developed an angular-dependent potential (ADP) for the W-Mo-Nb ternary system, which describes many important properties of pure metals and complex concentrated alloys with good accuracy [47]. Original article [47] contains a detailed validation of the developed potential and a comparison with available interatomic models for the W-Mo-Nb system: EAM [48–50], MEAM [51,52], SNAP [53], MTP [54], and tabGAP [55]. Among all tested models, only ADP and tabGAP proved to be suitable for the simulation of the bulk self-diffusion in pure metals, since only these two models can reproduce key properties with sufficient accuracy. Required characteristics include the vacancy formation energy E_{v0}^f, the vacancy migration energy E_v^m, and the melting temperature T_m. Here, in addition to the vacancy migration in pure metals, we calculated E_v^m during the exchange of the vacancy with a solute atom (i.e., the migration energy of an ω_2-type jump in the nine-jump model; see below).

Figure 1 shows the calculated values of E_v^m for ADP, tabGAP, MTP, and SNAP together with the available DFT results [5,6,43,44]. The figure shows only the migration energies for which we found the reference DFT values. More detailed information on the migration barriers can be found in the Supplemental Material [56]. It can be seen that SNAP and MTP significantly overestimate E_v^m compared to the DFT data. On the other hand, the ADP and tabGAP potentials correctly predict the hierarchy of diffusion barriers, despite the fact that the vacancy migration energies differ from the reference values by about 0.2 eV on average. Since ADP is five to six times faster than tabGAP and calculates E_{v0}^f more accurately [47], the former was chosen to study diffusion in this work. Some temperature dependencies shown here are given for homologous temperatures with T_m calculated in the original article [47]. All simulations were performed with the LAMMPS molecular dynamics simulator [57].

B. Static calculation

The diffusion coefficients of host and impurity atoms were calculated using Le Claire's nine-frequency model (nine-jump model) [58]; see Fig. 2. This model is based on calculating the jump frequencies, ω_i, for various atoms near a vacancy at given temperature T. For pure metals with a bcc lattice, the effective vacancy diffusion coefficient D_v is expressed as follows:

$$D_v = f_0 a^2 \omega_0, \tag{1}$$

where a is the lattice parameter and $f_0 = 0.727$ is the correlation factor [59,60]. The self-diffusion coefficient is equal to $D_v \cdot C_v$ with $C_v = \exp\left[(TS_{v0}^f - E_{v0}^f)/k_B T\right]$, where k_B is the Boltzmann constant and S_{v0}^f is the vacancy formation entropy.

The calculation of impurity diffusion requires taking into account multiple atomic jumps near the vacancy position.

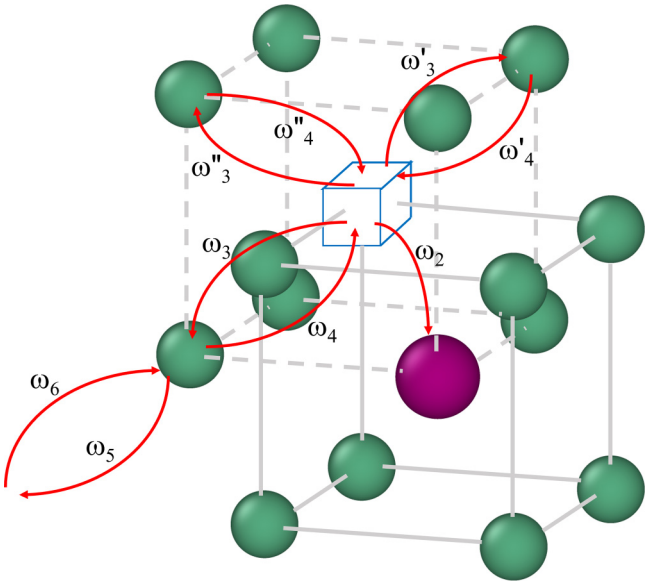

FIG. 2. Nine vacancy jumps distinguished according to the Le Claire model [58]. The green spheres represent the matrix atoms. A vacancy and an impurity atom in a nearest-neighbor configuration are shown by an empty box and a violet sphere, respectively. ω_2 corresponds to the vacancy–impurity atom exchange, ω_3/ω_4, ω_3'/ω_4', ω_5/ω_6, and ω_3''/ω_4'' represent the back/forth vacancy jumps to the second, third, fourth, and fifth neighbors of the impurity atom, respectively, and ω_0 is the jump frequency of all other possible vacancy jumps between nearest-neighbor positions (also, $\omega_6 = \omega_0$ according to this model).

Thus the impurity diffusion coefficient, D_2, is given by

$$D_2 = f_2 a^2 \omega_2 \frac{\omega_4}{\omega_3} C_v. \tag{2}$$

Here, f_2 is the correlation factor for impurity diffusion, described in terms of the nine-jump frequency model [61]

$$f_2 = \frac{1 - t_1}{1 + t_1}, \tag{3}$$

with

$$t_1 = \frac{\omega_2}{\omega_2 + 3\omega_3 + 3\omega_3' + \omega_3'' - t_2}, \tag{4}$$

$$t_2 = \frac{\omega_3 \omega_4}{\omega_4 + F\omega_5} + \frac{2\omega_3'\omega_4'}{\omega_4' + 3F\omega_0} + \frac{\omega_3''\omega_4''}{\omega_4'' + 5F\omega_0}, \tag{5}$$

and the factor $F = 0.512$.

The jump frequencies were estimated as

$$\omega_i = \nu_0 \exp\left(-\frac{E_i^m}{k_B T}\right), \tag{6}$$

where ν_0 is the Debye frequency for the given host and E_i^m is the migration barrier. Fifteen images between the initial and final configurations were considered for the energy barrier calculations using the climb image nudged elastic band method [62]. The determined energy barriers are listed in Table SI in the Supplemental Material.

For pure metals, the vacancy formation entropy S_{v0}^f was calculated using the PHONOPY code [63]. The calculation was based on the phonon entropies S_{id} and S_{vac} obtained at $T_0 = 300$ K for two simulated systems. The entropy S_{id} is related to the perfect crystal with 432 atoms in a simulation cell and S_{vac} is for the crystal with one vacancy (431 atoms in a simulation cell). From the difference between S_{vac} and the properly rescaled value of the entropy for the perfect crystal, $S_{id} \cdot (431/432)$, we estimated $S_{v0}^f = 2.0k_B$ for Mo and Nb and $S_{v0}^f = 2.7k_B$ for W. These values are consistent with the vacancy formation entropies calculated for bcc metals in other works [13,14,64].

For the CCAs, the averaged values of E_{v0}^f reflecting different local atomic environments were calculated in the spirit of the recent work [33]. The simulation cells contained N atoms forming a bcc random alloy (i.e., without taking into account short-range order) with different random number generator seeds for various compositions. For each composition, E_{v0}^f was calculated as

$$E_{v0}^f = \frac{\left(\sum_{i=1}^N E_i\right) - (N-1)E_0}{N}, \tag{7}$$

where E_0 is the energy of the perfect crystal (with N atoms) and E_i is the energy of the crystal with a single vacancy located at the ith site (with a total of $N-1$ atoms in the cell). In this way, the calculated E_{v0}^f can be considered as an average value over local chemical configurations for the given alloy composition. For a detailed discussion of the vacancy formation energy in multicomponent alloys, the reader is referred, e.g., to the recent paper of Zhang *et al.* [65]. The simulated crystals were relaxed with a force tolerance of 10^{-4} eV/Å. The number of atoms $N = 250$ was sufficient to obtain smooth composition dependences of E_{v0}^f with the points scattering less than 0.01 eV.

C. MD simulation of a single vacancy

A series of finite-temperature MD simulations were performed for a computational cell containing 249 atoms (i.e., 250 atoms arranged in a bcc lattice with a single vacancy). Each calculation was performed in the NPT ensemble (Nose-Hoover thermostat/barostat) with the volume adjusted to obtain zero pressure. The purpose of this study was to calculate the diffusion coefficients for a single vacancy D_v in pure metals and a ternary equiatomic alloy (with different random number seeds for different temperatures). The same calculations were used to estimate the temperature dependence of E_v^f in pure metals. Thus several additional calculations were performed for perfect crystals to obtain the energies of the reference states.

The effective vacancy diffusion coefficient was extracted from the sum of the squared displacements (δr_i^2) of all N atoms in the simulated system during the calculation time t, using the following equation:

$$D_v = \sum_{i=1}^{N} \delta r_i^2 / 6t. \tag{8}$$

Note that D_v describes the diffusion of all atoms in the presence of a single vacancy. For this reason, the vacancy diffusion correlation factor [66] is already included in the defined D_v. We found that MD time lengths of 4 ns are sufficient for a reliable determination of D_v at high temperatures, while

much longer times (of up to 20 ns) are required to achieve a sufficient number of jump events at lower temperatures.

D. Large-scale MD modeling

The most computationally expensive method in this work is large-scale MD modeling. The basic idea is that the concentration of point defects in a large simulated crystal containing a source of defects should reach an equilibrium value after an annealing stage (which can be relatively long). Due to the high computational cost, this method was initially used only at $T \approx T_m$ for a crystal coexisting with a liquid phase [67]. Then, as computing power developed, Mendelev *et al.* [68,69] applied such an approach to calculate C_v in bcc metals (Fe and β-Zr) with free surfaces for the temperature range of $T > 0.8T_m$. A particular advantage of this method is the possibility to obtain the equilibrium defect concentration at high temperature without prior knowledge of primary diffusion mechanisms and anharmonicity effects. Such a numerical experiment automatically captures the anharmonicity of atomic vibrations and other entropy-temperature effects with the only exception of electronic excitation, which is neglected compared to other factors [16,17]. This method has often been used to study the self-diffusion of atoms within a bulk [13,70] and along various extended crystal defects [45,46,71,72] in pure metals. Here, we applied such method to study diffusion in alloys.

The simulated crystal consisted of 673 200 atoms. The zero-pressure barostat and periodic boundary conditions were applied only in the two directions (y and z). In the x direction, the simulated crystal was terminated by free surfaces (the distance between the surfaces was $60a$). The dimensions of the simulated crystal in the y and z directions were $75a$. The Nosé-Hoover thermostat/barostat was used to maintain the simulation conditions. Vacancy concentration and diffusion coefficients were calculated only for atoms located in a bulk inner region of the crystal (diffusion region), more than 3 nm away from the free surfaces. The simulation consists of two successive stages: the annealing stage and the main MD run. The annealing stage is necessary to achieve the equilibrium concentration of vacancies inside the diffusion region. The annealing times depended on temperature/composition and varied in the range of 10 to 50 ns. The diffusion coefficients and equilibrium vacancy concentrations were estimated from the main MD run, the time of which varied in the range of 3 to 10 ns. The diffusion coefficients were calculated from the time dependence of the mean-square displacement of all atoms in the diffusion region after the annealing stage. The number of vacancies in the diffusion region was calculated by analyzing the time-averaged coordination number of the atoms. Also, after each MD simulation, the simulated crystal was subjected to faster quenching (with a cooling rate of 150 K/ps) and minimization to obtain a static configuration with minimum energy. These quenched configurations were analyzed with the OVITO software [73] to double-check the equilibrium value of C_v. In some cases (mostly for pure Nb), the C_v after minimization was 10–20% higher than the value obtained in the MD due to the limitations of the used analysis method. A possible reason for this difference is the fact that the displacements of atoms around vacancy in Nb are higher than in other studied metals due to the small migration barrier and the small elastic modulus C_{44}. Thus not all vacancies in Nb can be monitored by the used analysis method at high temperatures. Due to this verification, the concentrations obtained in MD were adjusted by the corresponding factor.

III. BEHAVIOR OF A SINGLE VACANCY

A. Diffusion of a single vacancy

Since atomic diffusion in the studied systems is controlled by the migration of vacancies, we first estimate the temperature dependence of D_v. Figure 3 shows the comparison of the D_v predicted in the static calculations for pure metals with the values calculated in the direct MD. The two methods generally agree, but for W and Mo the static method predicts D_v two to three times lower than the direct MD modeling. This small difference is probably due to anharmonic effects in the atomic vibrations [16]. For Nb, the statics and MD results are in a very good agreement, likely because the migration of vacancies in Nb is least affected by the anharmonicity [9,74].

In addition to the results for pure metals, Fig. 3 also shows the obtained dependence $D_v(T)$ for the ternary equiatomic WMoNb (or WMN) alloy. The calculation of the vacancy diffusion in CCAs using static methods is not a trivial task due to the large variety of microscopic states. Therefore, only values calculated in MD are shown in Fig. 3. It can be seen that the migration of a vacancy in the simulated CCA is enhanced compared to the diffusion in pure metals. The D_v calculated for the WMN alloy is three times higher than the geometric mean (GM) of the values in pure metals, which contradicts the concept of the sluggish diffusion effect in CCAs. Thus, at least for this temperature range ($T > 0.5T_m$), we can conclude that there is no sluggish diffusion for vacancy in the bcc WMN alloy. At lower temperatures than considered here, the sluggish diffusion might exist due to the presence of strong correlations in atomic jumps [75], but in our study we did not find the strong effect of such correlations on D_v.

B. Formation energy of single vacancy

The equilibrium vacancy concentration in pure metals is determined by the equation $C_v = \exp(-G_v^f/k_BT)$, where G_v^f is the Gibbs free energy of vacancy formation. In the case of zero pressure, this energy can be described to a first approximation as $G_v^f = E_{v0}^f - T \cdot S_{v0}^f$, where E_{v0}^f and S_{v0}^f are values calculated in the static calculations. However, previous studies with classical potentials [13,68,69,76,77] and first-principles methods [11,16,78] have shown that the vacancy formation energy/entropy can be strongly influenced by the temperature-induced anharmonicity, which leads to non-Arrhenius temperature dependence of C_v. Thus, for a more accurate calculation, it is necessary to take into account the change in the vacancy energy during heating.

The temperature dependences of E_v^f calculated in the MD simulation for all three metals are plotted in Fig. 4. The most significant increase in E_v^f upon heating was obtained for Mo, and the change in energy was proportional to T^4. As in our previous work [13], we calculated the temperature dependence of G_v^f by integrating the Gibbs-Helmholtz

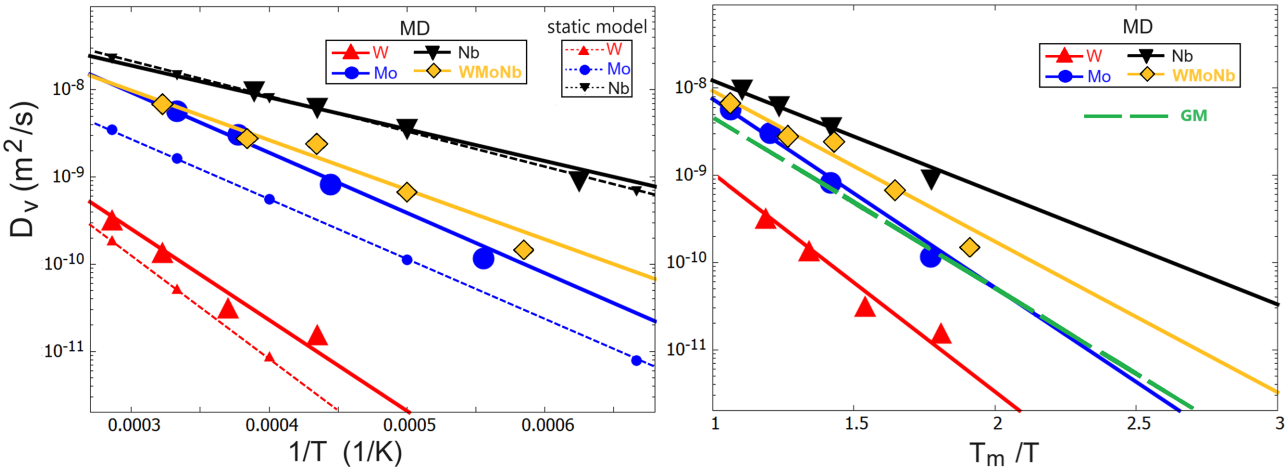

FIG. 3. Calculated temperature dependences of vacancy diffusion coefficients in pure metals and ternary equiatomic alloy. The results are given for absolute (left panel) and homologous temperatures (right panel). For absolute temperature, MD simulation results (large symbols) are compared with predictions based on the static calculations (small symbols). For homologous temperature, the green dashed line indicates GM of the values in the pure metals.

equation:

$$\frac{G_v^f(T)}{T} = \frac{E_{v0}^f - T_0 S_{v0}^f}{T_0} - \int_{T_0}^{T} \frac{E_v^f(T')}{T'^2} dT',$$

where T_0 is a reference temperature (taken as 300 K). Figure 4 shows the calculated dependencies $G_v^f(T)$ along with recent data obtained for W using *ab initio*–based machine learning (ML) calculations [16]. The small difference between the ADP-MD and ML results is mainly due to the difference in E_{v0}^f.

The formation energies of vacancies in alloys were calculated using the static approach only. The calculated energies are shown in Fig. 5. Together with the prediction of the ADP model, the figure includes the reference DFT values for pure metals [79]. The ADP potential predicts a nonmonotonic dependence of E_{v0}^f on the composition for Nb-based alloys. To the best of our knowledge, there are no DFT calculations available to confirm or refute such an effect. However, a recent study [80] revealed that several advanced ML potentials (MTP and SNAP) predict a significant softening of the bulk modulus for W-Nb alloys (for the high Nb region) and no such softening for W-Mo and W-Ta alloys. This softening can be interpreted as an indirect confirmation of the observed decrease in E_{v0}^f for the high Nb region of CCAs.

The vacancy formation energy in the ternary equiatomic alloy (2.91 eV) practically coincides with E_{v0}^f for pure Mo (2.88 eV). Also, the calculated melting temperatures are very close [47]: 3190 K and 3250 K for Mo and WMN alloy, respectively. Due to this similarity, the WMN alloy can be conveniently compared with pure Mo.

IV. LARGE-SCALE SIMULATION

The atomistic study of diffusion in CCA is quite challenging due to the large chemical diversity in the arrangement of atoms around a vacancy. Such states are characterized by different energy/entropy values and the cumulative effect of such diversity requires nontrivial consideration. Moreover, the properties of such configurations can strongly depend on temperature. In this case, large-scale MD simulation has a significant advantage over other methods because it can provide a uniform way of modeling with the same level of accuracy for pure metals, dilute alloys, and CCAs.

Figure 6 shows the examples of the large-scale simulation: snapshots of the initial annealing stage and the kinetics of

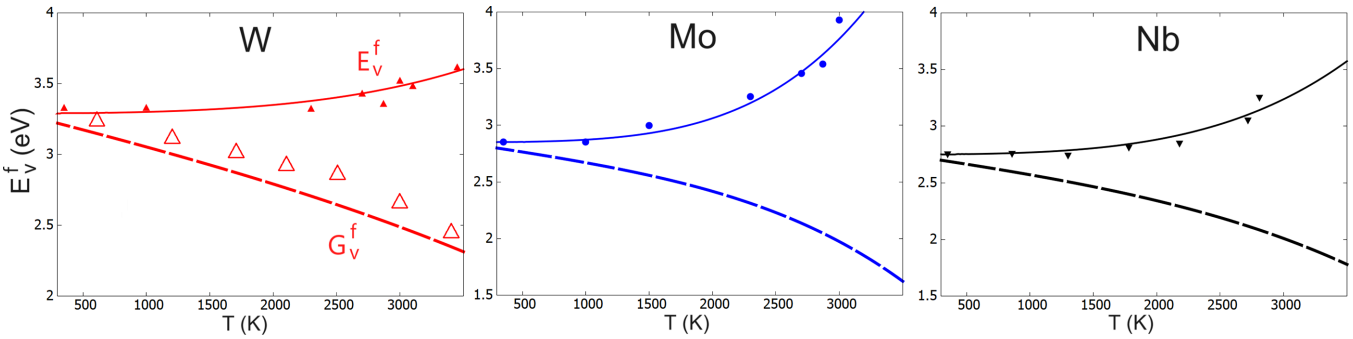

FIG. 4. Calculated temperature dependence of the vacancy formation energies in pure metals: solid lines and dashed lines correspond to energies E_v^f and G_v^f, respectively. The obtained results for W are compared with the prediction based on the *ab initio* ML approach [16].

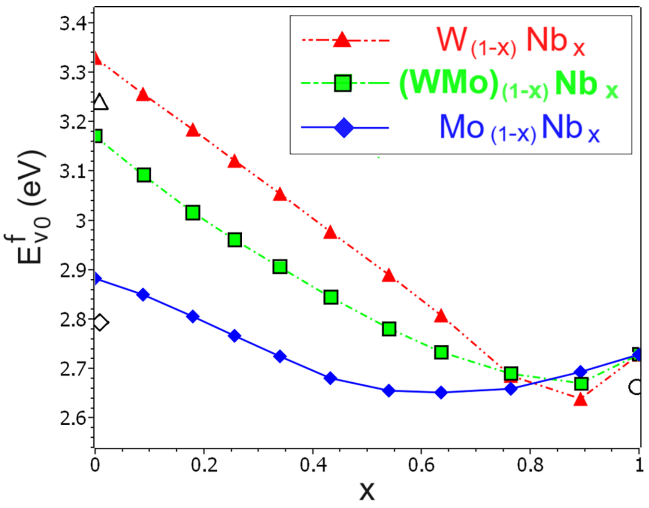

FIG. 5. Vacancy formation energy depending on alloy composition: the calculation results are given for two binary alloys (W-Nb and Mo-Nb) and ternary alloy $(WMo)_{(1-x)}Nb_x$. Open symbols correspond to E^f_{v0} calculated with the DFT method for pure metals [79]: triangle—W; diamond—Mo; circle—Nb.

vacancy accumulation in the diffusion region. These snapshots illustrate how surfaces emit vacancies into the bulk. Based on the simulation results for the annealing stage, the time required to reach the equilibrium concentration can be estimated as $t_{an} = 3 \cdot l^2/D_v$, where $l \approx 3.5$ nm is the distance between the surface and the diffusion region. The Supplemental Material [56] contains several typical dependencies of the mean square displacement of atoms within the diffusion region on time after the annealing stage. A few calculations were performed for pure metals and binary alloys, but most calculations were carried out for ternary alloys (dilute and CCA). In the case of a dilute alloy, the concentration of alloying elements was equal to 0.1 at.% and such a small number of substitution atoms does not affect C_v. Thus the calculated diffusion coefficients of matrix atoms in the dilute alloys can be considered as the self-diffusion coefficients in pure metals. This conclusion is supported by the results of the static calculations which predict moderate vacancy–impurity atom interactions, i.e., similar energy barriers for the type 3 and type 4 jumps; see Table SI in the Supplemental Material [56].

It is important to note here that we observed the formation of a partial chemical order in the large-scale simulations of CCA. The initial placement of atoms on the lattice had a random (uncorrelated) distribution. However, as vacancies were generated at the surface and wandered through the lattice exchanging atoms, a partial short-range order (SRO) was formed. The presence of SRO in CCAs is a common phenomenon [81,82] that can effect the vacancy-atom interaction [83]. The appearance of the short-range order in our simulation can be monitored by the drop in the total potential energy of the simulated system. The energy decrease occurred in the first 2–4 ns of the annealing stage and was approximately 0.003–0.006 eV/atom depending on temperature. This minor ordering does not appear to affect the diffusion characteristics, but at lower temperatures the situation may be different and require a separate study.

In all of the simulations performed, the main mechanism of atomic diffusion was based on the migration of single vacancies. However, rare cases of local ringlike exchange in the form of formation/recombination of bound Frenkel pairs were also observed. This spontaneous formation of point defects inside the crystal is in good agreement with the main results of another numerical experiment [84] performed on initially defect-free crystals. This exchange mechanism makes a small contribution to the diffusion of atoms and the largest contribution was obtained for Nb (about 25% of the total atomic displacement at $T = T_m$).

Figure 7 summarizes the calculated C_v for dilute alloys and the WMN equiatomic alloy. Together with the results of the large-scale simulations, the figure shows an analytical prediction of C_v in the form of $\exp(-G^f_v/k_BT)$ with G^f_v calculated in MD modeling for the pure metals. This analytical dependence agrees very well with the results of the numerical experiments for the dilute alloys. This fact proves that a small number of substitution atoms does not affect C_v, at least for such high temperatures. According to the obtained data, the concentration of vacancies in the WMN alloy is significantly higher than in pure metals (this is especially evident from the graph with absolute temperature). As was mentioned, the WMN alloy can be conveniently compared to pure Mo due to the similarity of E^f_{v0}: the vacancy concentration in the WMN alloy is four to five times higher than in the pure metal. Perhaps this large increase in C_v for the CCA results from the configuration entropy contribution discussed in several papers [32,85].

The vacancy concentration at the melting point (C^{melt}_v) is often considered as one of the key characteristics describing the atomic diffusion [86–90]. Based on the results obtained in this work and our previous studies, we found that the calculated value of C^{melt}_v correlates with T_m predicted by the same interatomic potential. This correlation is shown in Fig. 8. Based on the calculations with the ADP, the figure shows the results for pure metals, binary equiatomic WMo, ternary WMN, and $W_5Mo_3Nb_4$ alloys. The figure also includes our previous calculations [13,14] for the same metals performed with other interatomic potentials: Nb with ADP (ADP-2021) [14]; Mo with MEAM potential [91] and ADP model (ADP-2018) [92]. In fact, Pearson's correlation factor between the calculated values of $\ln C^{\text{melt}}_v$ and T_m for pure metals is about 0.84, which indicates a relatively strong positive correlation. Thus the calculated C^{melt}_v for pure metals can be estimated as $C_{\text{fit}} \exp(T_m/T_{\text{fit}})$, where the fitting coefficients C_{fit} and T_{fit} are equal to 4×10^{-6} and 610 K, respectively. It is interesting that the calculated values of T_m and C^{melt}_v for pure bcc metals in the recent work [17] also agree well with this correlation dependence: C^{melt}_v for Ta, V, and Mo deviate by 20–30% from the values predicted by the obtained dependence and C^{melt}_v for W differ only by a factor of 2.

Together with the calculated data, Fig. 8 illustrates a scatter in the available experimental values of C^{melt}_v for pure metals [86–90]. According to the positron annihilation spectroscopy or resistivity measurements, C^{melt}_v for refractory metals varies from 10^{-4} to 10^{-3}, which is generally consistent with the calculated data. Here we did not include C^{melt}_v identified when analyzing the temperature dependence of specific heat capacity and thermal expansion [93]: these high values obtained for

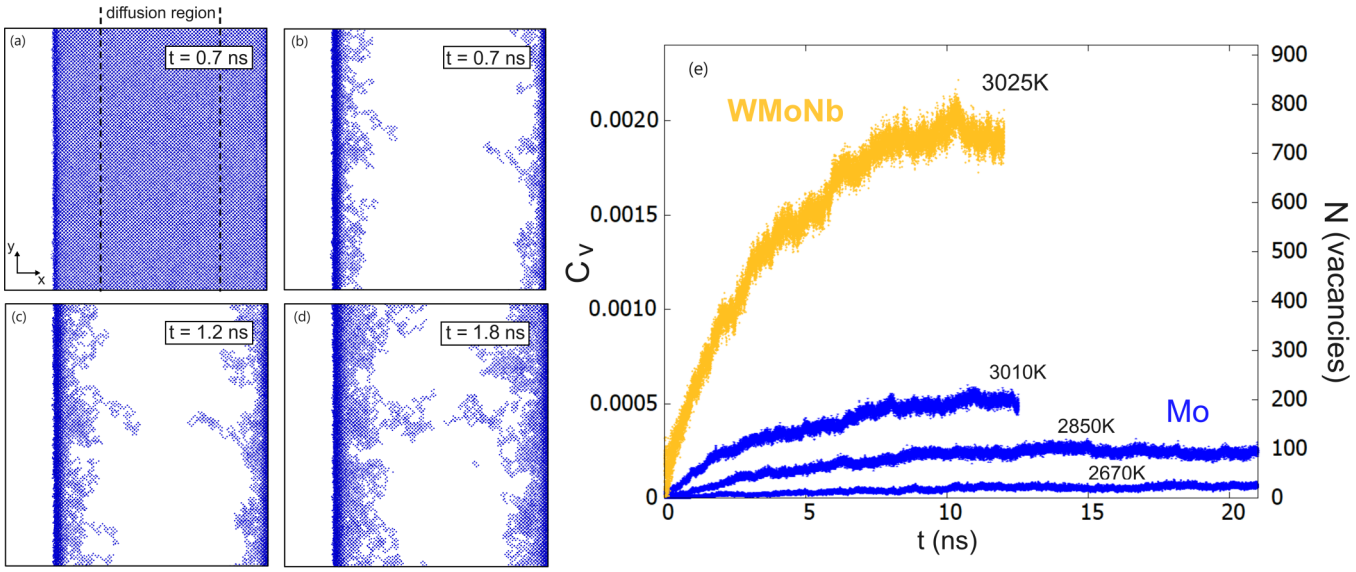

FIG. 6. (a)–(d) Snapshots of large-scale MD simulations of Mo at $T = 2850$ K during the first 1.8 ns of the modeling (the simulation time is shown in the snapshots). Panel (a) shows all simulated atoms. Panels (b)–(d) show the evolution of defects and their trajectories during the MD run: only atoms with the highest displacements ($\Delta r > 2.0$ Å) are shown. (e) The calculated dependence of C_v (left axis) and the number of vacancies N (right axis) in the diffusion region on the simulation time for pure Mo and ternary equiatomic alloy. The results are shown for different temperatures.

refractory metals (about 0.02–0.03) are probably linked with incorrect consideration of the lattice anharmonicity. A similar strong overestimation for C_v^{melt} takes place also for some thermodynamic models [94–96], probably for the same reason. As has been shown in a number of recent papers [17,97], a careful analysis of the anharmonic and electronic effects in refractory metals reconciles the measured heat capacity and thermal expansion with C_v^{melt} not exceeding 10^{-3}.

The most important feature of Fig. 8 for our analysis is the significant increase in C_v^{melt} for ternary CCAs compared to pure metals and even the binary alloy. An effect of the configurational entropy was thought to be responsible for such increase in the vacancy concentration in multicomponent alloys. Indeed, Wang *et al.* [32] found that C_v in a HEA consisting of n elements is greater than C_v in a pure metal having the same G_v^f by a factor of $\frac{\exp(n-1)}{n}$. During the derivation, vacancies were considered as $(n+1)$th element of the n-component alloy [32]. However, such a description does not preserve the chemical configuration of the alloy during vacancy formation, assuming implicitly that the elements can reorganize when vacancies are created [65]. A correct analysis of the vacancy energetics in HEAs predicted, e.g., an increase of the vacancy concentration in the ternary HfTiZr and quinary AlScHfTiZr hexagonal close-packed (hcp) alloys with respect to binary HfTi, while the vacancy concentration in the quaternary AlHfTiZr alloy is significantly decreased [65]. Those estimates

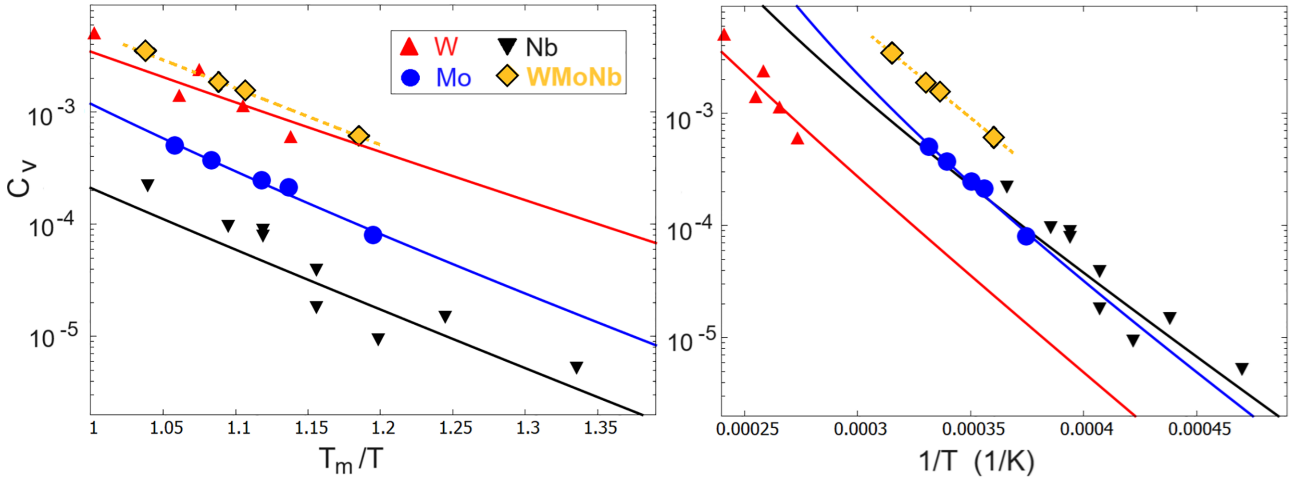

FIG. 7. Calculated temperature dependence of the equilibrium vacancy concentration. The symbols show the results of the direct large-scale MD simulations performed for dilute alloys and the ternary equiatomic alloy. The solid lines show the analytical function $C_v = \exp[-G_v^f/k_BT]$ for pure metals: black, blue, and red colors correspond to Nb, Mo, and W, respectively. The dashed line is a guide to the eye for the values obtained in the equiatomic alloy. The obtained results are given for homologous (left panel) and absolute temperatures (right panel).

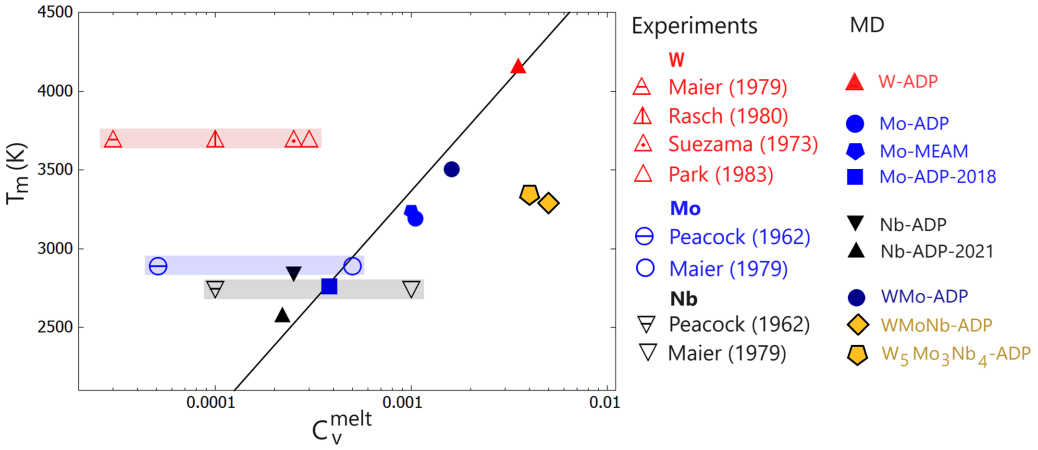

FIG. 8. Correlation plot between the simulated melting temperature and the vacancy concentration in this state. The figure contains the simulation results obtained with different interatomic potentials and the vacancy concentrations obtained from the experimental data for W [86–89], Mo [87,90], and Nb [87,90]. The three shaded regions indicate a scatter in the available experimental values. The black solid line corresponds to the relationship $C_{\text{fit}} \exp(T_m/T_{\text{fit}})$ discussed in the text.

for the hcp systems are largely consistent with our results for the refractory bcc alloys presented in Fig. 7.

All atomic diffusion coefficients calculated in the direct large-scale MD simulation are shown in Fig. 9 (three dilute alloys and WMN alloy). For the dilute alloys, Fig. 9 also shows the results of the static calculation. Namely, for the diffusion of A-type atoms in B matrix, the diffusion coefficient $D_{A(B)}$ was calculated using the nine-jump model and the vacancy concentration with the energy/entropy calculated for pure metal B. In addition, Fig. 9 shows the tracer diffusion coefficients D for pure metals calculated as $D_v \cdot \exp(-G_v^f/k_BT)$ with D_v and G_v^f obtained in the MD simulations with a single vacancy. Finally, Fig. 9 contains the measured diffusion coefficients in pure metals or dilute alloys [7,8,98–103]. This presentation of all the results in one figure gives us the opportunity to discuss several interesting patterns in the diffusion processes being studied.

By combining static simulations with MD modeling, we found that the hierarchy of elemental diffusion coefficients is the same for dilute and CCA systems: $D_{Nb} > D_{Mo} > D_W$. This trend agrees with the available experimental data (see Fig. 9). Only for the diffusion of W and Mo in the Nb matrix does the static modeling predict the inverse hierarchy $D_W > D_{Mo}$, in contrast to the MD modeling and the measured data. The reason for this difference probably lies in anharmonicity and more complex movement of atoms (like vacancy jump towards the next-nearest-neighbor positions [104]), which are not taken into account in the nine-jump model for these solutes. Moreover, in the case of W as impurity in the Nb matrix, the energy barrier for the ω_6 jumps, Fig. 2 in the manuscript and Table S1 in the Supplemental Material, deviates by about 7% from the ω_0 value, while such deviations are less than 3% for other impurity/matrix combinations. This fact indicates a limited applicability of the nine-jump model for W diffusion in Nb. Thus more distant vacancy jumps have to be included in the analysis with the corresponding refinement of the model. This may be a subject of a separate study. For all other cases, the hierarchy of the diffusion coefficients obtained with the static approaches agrees with the MD simulation. This uniform hierarchy valid for CCA is a very interesting fact that deserves a further study.

Another interesting aspect shown in Fig. 9 is a slight underestimation of the diffusion coefficients calculated by the static method compared to the MD simulations. This difference is due to two comparable factors: the underestimation of D_v (see Fig. 2) and the absence of non-Arrhenius behavior of C_v in the static calculations. The effect of non-Arrhenius behavior can be well illustrated by the example of D for Nb, since the values of D_v in static and MD calculations are basically identical: the solid (MD) and dashed (static) lines in Fig. 9 merge into a single dependence at low temperatures, when atomic anharmonicity disappears.

Figure 9 indicates one of the main conclusions of our work that the diffusion of atoms in CCA is enhanced compared to the atomic diffusion in the dilute alloys. This enhancement results from the increased values of D_v and C_v compared to the pure metals. To better illustrate this fact, we have plotted Fig. 10, where each panel combines all MD results for the same chemical element together with GM based only on atomic diffusion in dilute alloys. The calculated data in Fig. 10 also shows that the diffusion coefficients of the components in the equiatomic alloy are very close to the diffusion coefficients of the same elements in the Nb matrix. It is likely that diffusion in the alloy occurs in Nb-rich environments, since the diffusion barriers in the Nb matrix are lowest and these environments are probable enough to enable the diffusion process.

V. SLUGGISHNESS OF DIFFUSION IN MULTICOMPONENT ALLOYS

The sluggish diffusion concept has originally been introduced as a qualitative approach [19], without any quantification. Daw and Chandross [33] quantified this approach suggesting to relate the vacancy diffusion coefficients in an alloy with a geometric mean of the vacancy diffusion coefficients in pure elements (determined for the same crystalline lattice). Being straightforward and applicable for the

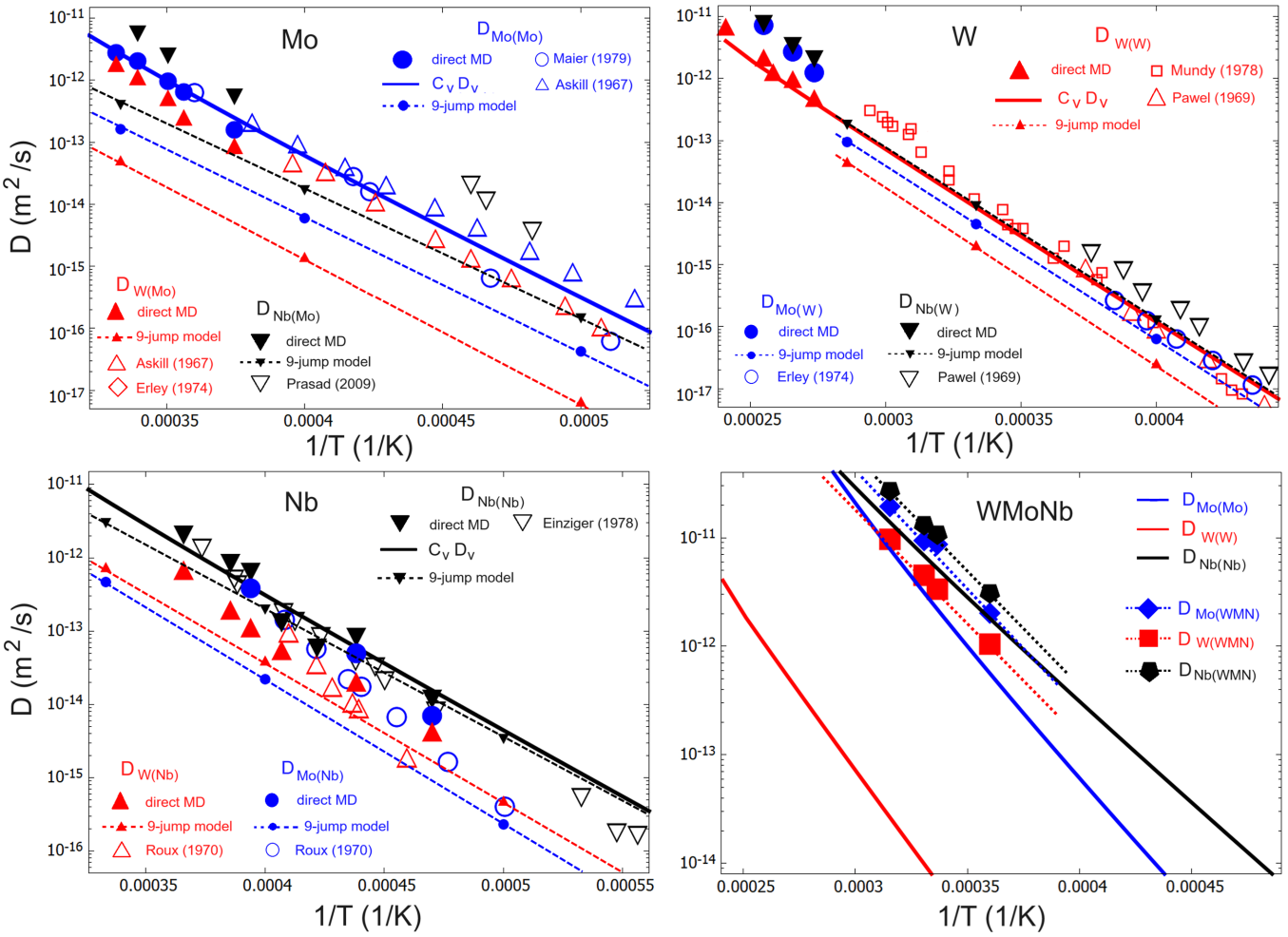

FIG. 9. Temperature dependence of the atomic diffusion coefficients in dilute alloys and ternary equiatomic alloy. Solid lines correspond to the self-diffusion $D = C_v \cdot D_v$ based on the MD results; dotted lines with small solid symbols indicate the impurity diffusion (and self-diffusion) obtained with the nine-jump model; the large solid symbols are the results of the large-scale MD simulation; large open symbols correspond to the measured coefficients [7,8,98–103]. For comparison, the panel with the results for the WMN alloy also contains the calculated D for pure metals.

atomistic simulation, see discussion above, such a comparison cannot be done using experimental data, since the vacancy diffusion rates are hardly to be measured [105]. In fact, a perturbed angular correlation can be used to determine the jump frequencies of atomic species and thus to estimate the vacancy diffusion coefficients in some systems [106,107], but such measurements require highly nontrivial approaches and suitable crystallographic lattices.

In order to circumvent this problem, Zhang *et al.* [31] and Sen *et al.* [34] suggested comparing the tracer diffusion

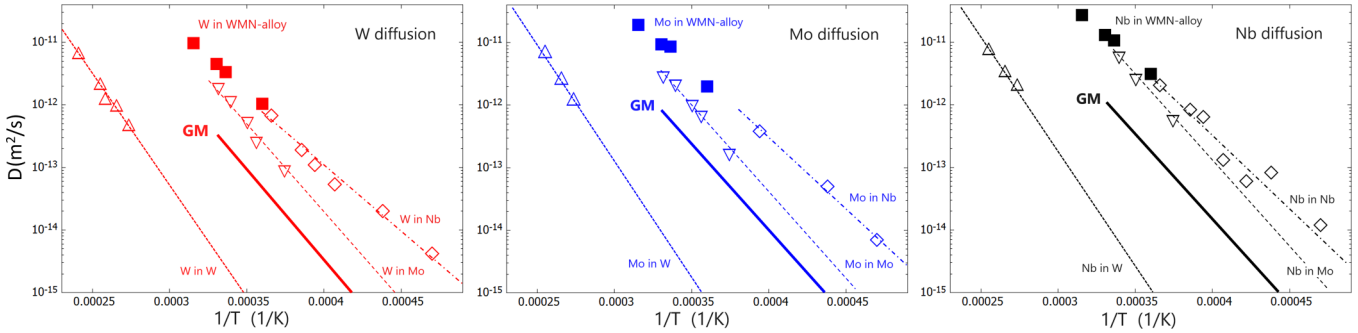

FIG. 10. Comparison of the calculated diffusion coefficients of a single metal in different matrices: open symbols—the results of the large-scale MD simulation in the dilute alloys; solid line—the geometric mean of the values in the dilute alloys; solid squares—the diffusion coefficients in the ternary equiatomic alloy calculated in the large-scale MD simulation.

coefficients of a given element in the alloy and in pure counterparts. This allowed a quantitative analysis of tracer diffusion in terms of potential chemical complexity-induced diffusion retardation/acceleration in HEAs or CCAs using the experimental data.

We evaluated the performance of the two approaches for the equatomic Mo–Nb–W alloy, Fig. 10. A "nonsluggishness" of diffusion of all constituting elements is observed following both vacancy and element-specific diffusion rates. We see that the tracer diffusion coefficients of all elements exceed those predicted by the geometric mean by an order of magnitude and a similar behavior is observed by comparison of the vacancy diffusion coefficients in pure elements and an equiatomic alloy. Note that a similar result was reported using the experimentally measured diffusion rates of Zr in bcc HfTiZrNbTa and the corresponding pure elements [31].

We conclude that the chemical complexity does not inevitably decrease the diffusion rates in compositionally complex alloys, in a clear contradiction to the original ideas. It is also important to note that we only focused on the relatively high temperatures ($T > 0.5T_m$) at which diffusion measurements are typically performed. It is possible that at lower temperatures the role of strong correlations in the atomic jumps may increase and the migration of vacancies can be suppressed. Note that kinks in the Arrhenius temperature dependence of the tracer diffusion coefficients were indeed reported for the fcc CoCrFeMnNi alloy [38] and they correlate with recorded changes of the dominant chemical environments of thermal vacancies in that system [108]. Such issues are left for further research.

ACKNOWLEDGMENTS

We are very grateful to the two reviewers for their reasonable questions and for their suggested corrections to improve the article. The calculations were carried out on the computer cluster Vulcan (ICAMS Computing cluster, RUB) and cluster Noctua2 of Paderborn Center for Parallel Computing (project "refall"). A partial financial support of the German Research Foundation, Project No. DI 1419/24-1, is acknowledged. S.S. gratefully acknowledges the financial support from the German Research Foundation, Project No. 453279121. P.G. acknowledges the support from the Cross-Disciplinary Program on Numerical Simulation of CEA, the French Alternative Energies and Atomic Energy Commission.

[1] A. Seeger, Diffusion and point-defect properties, in *Defect and Diffusion Forum* (Trans Tech Publ, Zurich, 1993), Vol. 95, pp. 147–170.

[2] H. Mehrer, *Diffusion in Solids: Fundamentals, Methods, Materials, Diffusion-Controlled Processes* (Springer Science & Business Media, New York, 2007), Vol. 155.

[3] J. Rogal, S. V. Divinski, M. W. Finnis, A. Glensk, J. Neugebauer, J. H. Perepezko, S. Schuwalow, M. H. Sluiter, and B. Sundman, Perspectives on point defect thermodynamics, Phys. Status Solidi B **251**, 97 (2014).

[4] A. Paul, T. Laurila, V. Vuorinen, and S. Divinski, *Thermodynamics, Diffusion and the Kirkendall Effect in Solids* (Springer Int. Publ., Zurich, Switzerland, 2014).

[5] S. long Wen, K. H. He, H. N. Cui, M. Pan, Z. Huang, and Y. Zhao, Migration properties of mono-vacancy in W-4*d*/5*d* transition metal alloys, J. Alloys Compd. **728**, 363 (2017).

[6] X.-s. Kong, K.-n. He, J. Hou, T. Zhang, and C. Liu, Trends in transition metal solute diffusion in metals: the case of tungsten, Comput. Mater. Sci. **179**, 109638 (2020).

[7] J. N. Mundy, S. J. Rothman, N. Q. Lam, H. A. Hoff, and L. J. Nowicki, Self-diffusion in tungsten, Phys. Rev. B **18**, 6566 (1978).

[8] R. E. Einziger, J. N. Mundy, and H. A. Hoff, Niobium self-diffusion, Phys. Rev. B **17**, 440 (1978).

[9] U. Köhler and C. Herzig, On the correlation between self-diffusion and the low-frequency LA $^2/_3$111 phonon mode in b.c.c. metals, Philos. Mag. A **58**, 769 (1988).

[10] G. Neumann and V. Tölle, Self-diffusion in body-centred cubic metals: Analysis of experimental data, Philos. Mag. A **61**, 563 (1990).

[11] A. Glensk, B. Grabowski, T. Hickel, and J. Neugebauer, Breakdown of the arrhenius law in describing vacancy formation energies: The importance of local anharmonicity revealed by ab initio thermodynamics, Phys. Rev. X **4**, 011018 (2014).

[12] X. Zhang, B. Grabowski, T. Hickel, and J. Neugebauer, Calculating free energies of point defects from ab initio, Comput. Mater. Sci. **148**, 249 (2018).

[13] D. Smirnova, S. Starikov, G. D. Leines, Y. Liang, N. Wang, M. N. Popov, I. A. Abrikosov, D. G. Sangiovanni, R. Drautz, and M. Mrovec, Atomistic description of self-diffusion in molybdenum: A comparative theoretical study of non-arrhenius behavior, Phys. Rev. Mater. **4**, 013605 (2020).

[14] S. Starikov and D. Smirnova, Optimized interatomic potential for atomistic simulation of Zr-Nb alloy, Comput. Mater. Sci. **197**, 110581 (2021).

[15] V. N. Maksimenko, A. G. Lipnitskii, V. N. Saveliev, I. V. Nelasov, and A. I. Kartamyshev, Prediction of the diffusion characteristics of the V-Cr system by molecular dynamics based on n-body interatomic potentials, Comput. Mater. Sci. **198**, 110648 (2021).

[16] X. Zhang, S. V. Divinski, and B. Grabowski, Ab initio machine-learning unveils strong anharmonicity in non-arrhenius self-diffusion of tungsten, arXiv:2311.00633.

[17] A. Forslund, J. H. Jung, P. Srinivasan, and B. Grabowski, Thermodynamic properties on the homologous temperature scale from direct upsampling: Understanding electron-vibration coupling and thermal vacancies in bcc refractory metals, Phys. Rev. B **107**, 174309 (2023).

[18] A. Dash, A. Paul, S. Sen, S. Divinski, J. Kundin, I. Steinbach, B. Grabowski, and X. Zhang, Recent advances in understanding diffusion in multiprincipal element systems, Annu. Rev. Mater. Res. **52**, 383 (2022).

[19] J.-W. Yeh, S.-K. Chen, S.-J. Lin, J.-Y. Gan, T.-S. Chin, T.-T. Shun, C.-H. Tsau, and S.-Y. Chang, Nanostructured high-entropy alloys with multiple principal elements: Novel alloy design concepts and outcomes, Adv. Eng. Mater. **6**, 299 (2004).

[20] K.-Y. Tsai, M.-H. Tsai, and J.-W. Yeh, Sluggish diffusion in Co–Cr–Fe–Mn–Ni high-entropy alloys, Acta Mater. **61**, 4887 (2013).

[21] M. C. Gao, J.-W. Yeh, P. K. Liaw, and Y. Zhang, *High-Entropy Alloys: Fundamentals and Applications* (Springer, New York, 2016).

[22] B. S. Murty, J.-W. Yeh, S. Ranganathan, and P. P. Bhattacharjee, *High-Entropy Alloys* (Elsevier, Amsterdam, 2019).

[23] G. M. Muralikrishna, V. A. Esin, K. N. Kulkarni, B. Murty, G. Wilde, and S. V. Divinski, Atomic transport in B2-ordered Al(Fe,Ni) alloys: Tracer-interdiffusion couple approach, Intermetallics **126**, 106920 (2020).

[24] J. Dabrowa, W. Kucza, G. Cieślak, T. Kulik, M. Danielewski, and J.-W. Yeh, Interdiffusion in the fcc-structured Al-Co-Cr-Fe-Ni high entropy alloys: Experimental studies and numerical simulations, J. Alloys Compd. **674**, 455 (2016).

[25] A. Roy, J. Munshi, and G. Balasubramanian, Low energy atomic traps sluggardize the diffusion in compositionally complex refractory alloys, Intermetallics **131**, 107106 (2021).

[26] X. Zhou, S. He, and J. Marian, Vacancy energetics and diffusivities in the equiatomic multielement Nb-Mo-Ta-W alloy, Materials **15**, 5468 (2022).

[27] J. Kottke, D. Utt, B. Laurent, A. Fareed, D. Gaertner, L. Perriere, Ł. Rogal, A. Stukowski, K. Albe, S. Divinski *et al.*, Experimental and theoretical study of tracer diffusion in a series of $(CoCrFeMn)_{100-x}Ni_x$ alloys, Acta Mater. **194**, 236 (2020).

[28] S. V. Divinski, A. V. Pokoev, N. Esakkiraja, and A. Paul, A mystery of sluggish diffusion in high-entropy alloys: The truth or a myth?, Diffus. Found. **17**, 69 (2018).

[29] A. Mehta and Y. H. Sohn, Fundamental core effects in transition metal high-entropy alloys: High-entropy and sluggish diffusion effects, Diffus. Found. **29**, 75 (2021).

[30] M. Zajusz, M. Jawańska, J. Dabrowa, K. Berent, G. Cieślak, T. Kulik, and K. Mroczka, Evaluation of phase stability and diffusion kinetics in novel bcc-structured high entropy alloys, Mater. Res. Lett. **10**, 556 (2022).

[31] J. Zhang, C. Gadelmeier, S. Sen, R. Wang, X. Zhang, Y. Zhong, U. Glatzel, B. Grabowski, G. Wilde, and S. V. Divinski, Zr diffusion in BCC refractory high entropy alloys: A case of non-sluggish diffusion behavior, Acta Mater. **233**, 117970 (2022).

[32] Z. Wang, C. T. Liu, and P. Dou, Thermodynamics of vacancies and clusters in high-entropy alloys, Phys. Rev. Mater. **1**, 043601 (2017).

[33] M. S. Daw and M. Chandross, Sluggish diffusion in random equimolar FCC alloys, Phys. Rev. Mater. **5**, 043603 (2021).

[34] S. Sen, X. Zhang, L. Rogal, G. Wilde, B. Grabowski, and S. V. Divinski, Anti-sluggish Ti diffusion in HCP high-entropy alloys: Chemical complexity vs. lattice distortions, Scr. Mater. **224**, 115117 (2023).

[35] D. Gärtner, L. Belkacemi, V. A. Esin, F. Jomard, A. A. Fedotov, J. Schell, J. V. Osinskaya, A. V. Pokoev, C. Duhamel, A. Paul, and S. V. Divinski, Techniques of tracer diffusion measurements in metals, alloys and compounds, Diffus. Found. **29**, 31 (2021).

[36] M. Vaidya, S. Trubel, B. S. Murty, G. Wilde, and S. V. Divinski, Ni tracer diffusion in CoCrFeNi and CoCrFeMnNi high entropy alloys, J. Alloys Compd. **688**, 994 (2016).

[37] M. Vaidya, K. Pradeep, B. Murty, G. Wilde, and S. Divinski, Bulk tracer diffusion in CoCrFeNi and CoCrFeMnNi high entropy alloys, Acta Mater. **146**, 211 (2018).

[38] D. Gaertner, J. Kottke, Y. Chumlyakov, F. Hergemöller, G. Wilde, and S. Divinski, Tracer diffusion in single crystalline CoCrFeNi and CoCrFeMnNi high-entropy alloys: Kinetic hints towards a low-temperature phase instability of the solid-solution?, Scr. Mater. **187**, 57 (2020).

[39] D. Gaertner, K. Abrahams, J. Kottke, V. Esin, I. Steinbach, G. Wilde, and S. Divinski, Concentration-dependent atomic mobilities in FCC CoCrFeMnNi high-entropy alloys, Acta Mater. **166**, 357 (2019).

[40] M. Vaidya, S. Sen, X. Zhang, L. Frommeyer, Ł. Rogal, S. Sankaran, B. Grabowski, G. Wilde, and S. Divinski, Phenomenon of ultra-fast tracer diffusion of Co in HCP high entropy alloys, Acta Mater. **196**, 220 (2020).

[41] S. Sen, X. Zhang, L. Rogal, J. Schell, G. Wilde, B. Grabowski, and S. V. Divinski, Sc diffusion in Hcp high entropy alloys, Scr. Mater. **242**, 115917 (2024).

[42] J. Zhang, G. Muralikrishna, A. Asabre, Y. Kalchev, J. Müller, B. Butz, S. Hilke, H. Rösner, G. Laplanche, S. Divinski *et al.*, Tracer diffusion in the σ phase of the CoCrFeMnNi system, Acta Mater. **203**, 116498 (2021).

[43] P.-W. Ma and S. L. Dudarev, Effect of stress on vacancy formation and migration in body-centered-cubic metals, Phys. Rev. Mater. **3**, 063601 (2019).

[44] N. Zou, H.-J. Lu, and X.-G. Lu, Impurity diffusion coefficients in bcc nb from first-principles calculations, J. Alloys Compd. **803**, 684 (2019).

[45] S. Starikov, M. Mrovec, and R. Drautz, Study of grain boundary self-diffusion in iron with different atomistic models, Acta Mater. **188**, 560 (2020).

[46] S. Starikov, V. Jamebozorgi, D. Smirnova, R. Drautz, and M. Mrovec, Atomistic simulations of pipe diffusion in bcc transition metals, Acta Mater. **260**, 119294 (2023).

[47] S. Starikov, P. Grigorev, and P. A. Olsson, Angular-dependent interatomic potential for large-scale atomistic simulation of w-mo-nb ternary alloys, Comput. Mater. Sci. **233**, 112734 (2024).

[48] X. Zhou, H. Wadley, R. A. Johnson, D. Larson, N. Tabat, A. Cerezo, A. Petford-Long, G. Smith, P. Clifton, R. Martens *et al.*, Atomic scale structure of sputtered metal multilayers, Acta Mater. **49**, 4005 (2001).

[49] X. W. Zhou, R. A. Johnson, and H. N. G. Wadley, Misfit-energy-increasing dislocations in vapor-deposited CoFe/NiFe multilayers, Phys. Rev. B **69**, 144113 (2004).

[50] D.-Y. Lin, S. S. Wang, D. L. Peng, M. Li, and X. D. Hui, An n-body potential for a Zr–Nb system based on the embedded-atom method, J. Phys.: Condens. Matter **25**, 105404 (2013).

[51] B.-J. Lee, M. I. Baskes, H. Kim, and Y. K. Cho, Second nearest-neighbor modified embedded atom method potentials for bcc transition metals, Phys. Rev. B **64**, 184102 (2001).

[52] S.-P. Ju, C.-C. Li, and H.-T. Shih, How atoms of polycrystalline $Nb_{20.6}Mo_{21.7}Ta_{15.6}W_{21.1}V_{21.0}$ refractory high-entropy alloys rearrange during the melting process, Sci. Rep. **12**, 5183 (2022).

[53] X.-G. Li, C. Chen, H. Zheng, Y. Zuo, and S. P. Ong, Complex strengthening mechanisms in the NbMoTaW multi-principal element alloy, npj Comput. Mater. **6**, 70 (2020).

[54] S. Yin, Y. Zuo, A. Abu-Odeh, H. Zheng, X.-G. Li, J. Ding, S. P. Ong, M. Asta, and R. O. Ritchie, Atomistic simulations of dislocation mobility in refractory high-entropy alloys and the effect of chemical short-range order, Nat. Commun. **12**, 4873 (2021).

[55] J. Byggmästar, K. Nordlund, and F. Djurabekova, Simple machine-learned interatomic potentials for complex alloys, Phys. Rev. Mater. **6**, 083801 (2022).

[56] See Supplemental Material at http://link.aps.org/supplemental/10.1103/PhysRevMaterials.8.043603 for description calculated migration barriers and time dependences of MSD.

[57] S. Plimpton, Fast parallel algorithms for short-range molecular dynamics, J. Comput. Phys. **117**, 1 (1995).

[58] A. D. L. Claire, Solvent self-diffusion in dilute b.c.c. solid solutions, Philos. Mag. **21**, 819 (1970).

[59] K. Compaan and Y. Haven, Correlation factors for diffusion in solids, Trans. Faraday Soc. **52**, 786 (1956).

[60] G. L. Montet, Integral methods in the calculation of correlation factors in diffusion, Phys. Rev. B **7**, 650 (1973).

[61] A. D. L. Claire, in *Physical Chemistry: An Advanced Treatise*, edited by W. H. Eyring and D. Henderson (Academic Press, Inc., New York, 1970), Vol. X, Chap. 5.

[62] G. Henkelman and H. Jonsson, Improved tangent estimate in the nudged elastic band method for finding minimum energy paths and saddle points, J. Chem. Phys. **113**, 9978 (2000).

[63] A. Togo and I. Tanaka, First principles phonon calculations in materials science, Scr. Mater. **108**, 1 (2015).

[64] S. Starikov, D. Smirnova, T. Pradhan, Y. Lysogorskiy, H. Chapman, M. Mrovec, and R. Drautz, Angular-dependent interatomic potential for large-scale atomistic simulation of iron: Development and comprehensive comparison with existing interatomic models, Phys. Rev. Mater. **5**, 063607 (2021).

[65] X. Zhang, S. V. Divinski, and B. Grabowski, Ab initio prediction of vacancy energetics in HCP Al-Hf-Sc-Ti-Zr high entropy alloys and the subsystems, Acta Mater. **227**, 117677 (2022).

[66] Note that the vacancy correlation factor in an alloy is less than unity when the jumps' frequencies of the constituents are different [2]. Thus the vacancy jumps are not fully random, since the exchanges with some atom types are more likely.

[67] K. Nordlund and R. S. Averback, Role of self-interstitial atoms on the high temperature properties of metals, Phys. Rev. Lett. **80**, 4201 (1998).

[68] M. I. Mendelev and Y. Mishin, Molecular dynamics study of self-diffusion in bcc Fe, Phys. Rev. B **80**, 144111 (2009).

[69] M. I. Mendelev and B. S. Bokstein, Molecular dynamics study of self-diffusion in Zr, Philos. Mag. **90**, 637 (2010).

[70] D. Smirnova, S. Starikov, and I. Gordeev, Evaluation of the structure and properties for the high-temperature phase of zirconium from the atomistic simulations, Comput. Mater. Sci. **152**, 51 (2018).

[71] T. Frolov and Y. Mishin, Molecular dynamics modeling of self-diffusion along a triple junction, Phys. Rev. B **79**, 174110 (2009).

[72] S. Starikov, A. Abbass, R. Drautz, and M. Mrovec, Disordering complexion transition of grain boundaries in bcc metals: Insights from atomistic simulations, Acta Mater. **261**, 119399 (2023).

[73] A. Stukowski, Visualization and analysis of atomistic simulation data with ovito–the open visualization tool, Modell. Simul. Mater. Sci. Eng. **18**, 015012 (2010).

[74] F. Guthoff, B. Hennion, C. Herzig, W. Petry, H. Schober, and J. Trampenau, Lattice dynamics and self-diffusion in niobium at elevated temperatures, J. Phys.: Condens. Matter **6**, 6211 (1994).

[75] B. Xing, W. Zou, T. J. Rupert, and P. Cao, Vacancy diffusion barrier spectrum and diffusion correlation in multicomponent alloys, Acta Mater. **266**, 119653 (2024).

[76] L. Zhao, R. Najafabadi, and D. J. Srolovitz, Finite temperature vacancy formation thermodynamics: Local harmonic and quasiharmonic studies, Modell. Simul. Mater. Sci. Eng. **1**, 539 (1993).

[77] N. Sandberg and G. Grimvall, Anharmonic contribution to the vacancy formation in Cu, Phys. Rev. B **63**, 184109 (2001).

[78] T. R. Mattsson, N. Sandberg, R. Armiento, and A. E. Mattsson, Quantifying the anomalous self-diffusion in molybdenum with first-principles simulations, Phys. Rev. B **80**, 224104 (2009).

[79] P.-W. Ma and S. L. Dudarev, Universality of point defect structure in body-centered cubic metals, Phys. Rev. Mater. **3**, 013605 (2019).

[80] A. Al Mamun, S. Xu, X.-G. Li, and Y. Su, Comparing interatomic potentials in calculating basic structural parameters and peierls stress in tungsten-based random binary alloys, Phys. Scr. **98**, 105923 (2023).

[81] J. M. Cowley, An approximate theory of order in alloys, Phys. Rev. **77**, 669 (1950).

[82] N. Norman and B. E. Warren, X-Ray measurement of short range order in Ag-Au, J. Appl. Phys. **22**, 483 (1951).

[83] V. Kulitckii, O. Lukianova, A. Schneider, G. Wilde, C.-C. Fu, and S. V. Divinski, Atomic diffusion in bcc Fe–Mn alloys: Theoretical analysis and experimental measurements across the Curie temperature, Acta Mater. **251**, 118883 (2023).

[84] E. Fransson and P. Erhart, Defects from phonons: Atomic transport by concerted motion in simple crystalline metals, Acta Mater. **196**, 770 (2020).

[85] Z. Shen, J.-P. Du, S. Shinzato, Y. Sato, P. Yu, and S. Ogata, Kinetic monte carlo simulation framework for chemical short-range order formation kinetics in a multi-principal-element alloy, Comput. Mater. Sci. **198**, 110670 (2021).

[86] M. Suezawa and H. Kimura, Quenched-in vacancies in molybdenum, Philos. Mag. **28**, 901 (1973).

[87] K. Maier, M. Peo, B. Saile, H. Schaefer, and A. Seeger, High–temperature positron annihilation and vacancy formation in refractory metals, Philos. Mag. A **40**, 701 (1979).

[88] K. Rasch, R. Siegel, and H. Schultz, Quenching and recovery investigations of vacancies in tungsten, Philos. Mag. A **41**, 91 (1980).

[89] J. Park, H. Huang, R. Siegel, and R. Balluffi, A quantitative study of vacancy defects in quenched tungsten by combined field-ion microscopy and electrical resistometry, Philos. Mag. A **48**, 397 (1983).

[90] D. Peacock and A. Johnson, Stage iii recovery in neutron irradiated molybdenum and niobium, Philos. Mag. **8**, 563 (1963).

[91] H. Park, M. R. Fellinger, T. J. Lenosky, W. W. Tipton, D. R. Trinkle, S. P. Rudin, C. Woodward, J. W. Wilkins, and R. G. Hennig, Ab initio based empirical potential used to study

the mechanical properties of molybdenum, Phys. Rev. B **85**, 214121 (2012).

[92] S. Starikov, L. Kolotova, A. Y. Kuksin, D. Smirnova, and V. Tseplyaev, Atomistic simulation of cubic and tetragonal phases of U-Mo alloy: Structure and thermodynamic properties, J. Nucl. Mater. **499**, 451 (2018).

[93] Y. Kraftmakher, Equilibrium vacancies and thermophysical properties of metals, Phys. Rep. **299**, 79 (1998).

[94] Y. Tang and L. Zhang, Effect of thermal vacancy on thermodynamic behaviors in bcc W close to melting point: A thermodynamic study, Mater. **11**, 1648 (2018).

[95] E. Zhang, Y. Tang, M. Wen, A. Obaied, I. Roslyakova, and L. Zhang, On phase stability of Mo-Nb-Ta-W refractory high entropy alloys, Int. J. Refract. Met. Hard Mater. **103**, 105780 (2022).

[96] A. Obaied, I. Roslyakova, and M. To Baben, Including state-of-the-art physical understanding of thermal vacancies in calphad models, Sci. Rep. **12**, 13385 (2022).

[97] J. H. Jung, P. Srinivasan, A. Forslund, and B. Grabowski, High-accuracy thermodynamic properties to the melting point from ab initio calculations aided by machine-learning potentials, npj Comput. Mater. **9**, 3 (2023).

[98] K. Maier, H. Mehrer, and G. Rein, Self-diffusion in molybdenum, Int. J. Mater. Res. **70**, 271 (1979).

[99] J. Askill, Tracer diffusion of tungsten in molybdenum, Phys. Status Solidi B **23**, K21 (1967).

[100] W. Erley and H. Wagner, The diffusion coefficients in the system molybdenum–tungsten, Phys. Stat. Solidi A **25**, 463 (1974).

[101] S. Prasad and A. Paul, Diffusion parameters in the Nb-Mo system: Revisited, Metall. Mater. Trans. A **40**, 1512 (2009).

[102] R. Pawel and T. Lundy, Tracer diffusion in tungsten, Acta Metall. **17**, 979 (1969).

[103] F. Roux and A. Vignes, Diffusion dans les systèmes Ti-Nb, Zr-Nb, V-Nb, Mo-Nb, W-Nb, Rev. Phys. Appl. (Paris) **5**, 393 (1970).

[104] J. Zhang, G. Chen, and K. Xu, Self-diffusion of BCC transition metals calculated with MAEAM, Phys. B: Condens. Matter **390**, 320 (2007).

[105] S. Divinski, Defects and diffusion in ordered compounds, *Handbook of Solid State Diffusion* (Elsevier, Amsterdam, 2017), Chap. 10, Vol. 1, p. 449.

[106] G. Collins, S. Shropshire, and J. Fan, Perturbed $\gamma - \gamma$ angular correlations: A spectroscopy for point defects in metals and alloys, Hyperfine Interact **62**, 1 (1990).

[107] M. O. Zacate and H. Jaeger, Perturbed angular correlation spectroscopy – A tool for the study of defects and diffusion at the atomic scale, Defect Diffus. Forum **311**, 3 (2011).

[108] A. Smekhova, D. Gaertner, A. Kuzmin, A. G. Buzanich, G. Schuck, I. Zizak, G. Wilde, K. V. Yusenko, and S. Divinski, Anomalies in the short-range local environment and atomic diffusion in single crystalline equiatomic CrMnFeCoNi high-entropy alloy, Nano Res. (2023), doi:10.1007/s12274-024-6443-6.